Energy dissipation in microfluidic beam resonators: Dependence on mode number

John E. Sader,[1,a)] Jungchul Lee,[2,b)] and Scott R. Manalis[2,3]
[1]*Department of Mathematics and Statistics, The University of Melbourne, Victoria 3010, Australia*
[2]*Department of Biological Engineering, Massachusetts Institute of Technology, Cambridge, Massachusetts 02139, USA*
[3]*Department of Mechanical Engineering, Massachusetts Institute of Technology, Cambridge, Massachusetts 02139, USA*

(Received 29 July 2010; accepted 13 October 2010; published online 9 December 2010)

Energy dissipation experienced by vibrating microcantilever beams immersed in fluid is strongly dependent on the mode of vibration, with quality factors typically increasing with mode number. Recently, we examined energy dissipation in a new class of cantilever device that embeds a microfluidic channel in its interior—the fundamental mode of vibration only was considered. Due to its importance in practice, we examine the effect of mode number on energy dissipation in these microfluidic beam resonators. Interestingly, and in contrast to other cantilever devices, we find that the quality factor typically decreases with increasing mode number. We explore the underlying physical mechanisms leading to this counterintuitive behavior, and provide a detailed comparison to experimental measurements for which good agreement is found. © *2010 American Institute of Physics*. [doi:10.1063/1.3514100]

I. INTRODUCTION

The sensitivity of nanomechanical devices to environmental changes, such as mass and force loading,[1–4] is controlled by numerous factors including device mass and energy dissipation (damping). To enhance sensitivity to loading by minute masses, significant effort has been directed at miniaturization to the nanoscale.[1,2] These developments have resulted in tremendous improvements,[1,2,5] with recent measurements demonstrating atomic resolution mass sensing of the heavier elements.[6,7] Such measurements monitor the change in resonant frequency of an elastic beam (e.g., carbon nanotube in Refs. 6 and 7) upon mass loading. Critically, these are typically performed in vacuum, which minimizes damping experienced by the beam. This ensures that frequency noise is kept to a minimum, leading to maximum mass sensitivity.[1,4–7]

In contrast to vacuum, operation of cantilever beam devices in liquid presents significant challenges, due to greatly enhanced energy dissipation.[8,9] This strongly decreases the quality factor (which is proportional to the reciprocal of the energy dissipation), and hence degrades both frequency and mass resolution. Such effects are especially problematic in the context of biomolecular and single cell mass sensing, where operation in liquid is essential for many cases of practical interest. In an attempt to overcome this impediment, a number of schemes have been proposed for operation of cantilever beams and nanomechanical devices in liquid.[10–12] One approach utilizes detection of the higher order modes of conventional cantilever beams,[10] since it is known that the quality factor typically increases with increasing mode number[8,10,13]—fluid compressibility can modify this behavior in gases.[14] While this presents significant improvements in comparison to operation in the fundamental mode, mass sensitivity remains dramatically lower than measurements in vacuum.

Recently, Burg *et al.*[15] developed a new type of cantilever sensor that embeds a microfluidic channel in its interior, with the region surrounding the cantilever evacuated—these devices are commonly called suspended microchannel resonators;[15,16] see Fig. 1. This results in a dramatic reduction in energy dissipation, and hence improvement in both quality factor and mass sensitivity. Quality factors similar to those exhibited by conventional cantilevers in vacuum were observed.[15,16] Mass measurements in liquid with femtogram

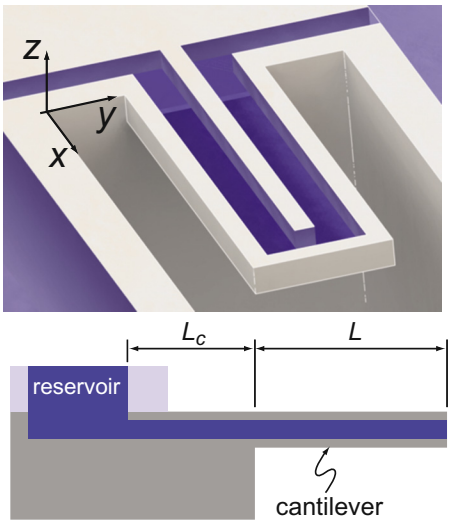

FIG. 1. (Color online) Illustration of fluid channel embedded microcantilever. Perspective (top): layout of the embedded fluid channel, which is normally closed and shown open here for illustration. Side view (bottom): cantilever structure (gray) showing cantilever length L and length of rigid lead channel L_c. Fluid channel is completely filled with fluid.

[a)]Electronic mail: jsader@unimelb.edu.au.
[b)]Current address: Department of Mechanical Engineering, Sogang University, Seoul 121-742, South Korea.

sensitivity were demonstrated originally,[15] with a recent article reporting sensitivity in the attogram range upon miniaturization to the nanoscale.[16]

Underpinning measurements using these microfluidic beam devices are their inherently high quality factors in the presence of liquid. Strikingly, it was observed[15] that the fundamental mode quality factor was unaffected when air or water was placed in the channel, with values of ~15 000 being achieved in both cases, for a single device. This is in direct contrast to conventional microcantilever devices immersed in fluid, which exhibit a strong decrease in quality factor upon immersion in air and liquid—typically, quality factors in vacuum, air and water are in the range of ~15 000, ~10–100, and ~1–2, respectively.[9,17,18] This unprecedented and inherent property of microfluidic beam devices was recently examined both experimentally and theoretically,[19,20] and was found to originate from dramatically different flow behavior in comparison to conventional cantilever devices.[9,10,13,14,21–24] In short, multiple flow regimes exist in these microfluidic devices, which can result in either an increase or decrease in energy dissipation with increasing fluid viscosity. At low viscosity (high inertia), a shear driven mechanism leads to increasing energy dissipation with increasing fluid viscosity. At intermediate to high viscosity, the viscous boundary layers overlap which yields the opposite behavior, i.e., energy dissipation falls with increasing viscosity. At high viscosity (low inertia), any off-axis placement of the channel away from the neutral axis of the beam gives rise to an additional pumping mechanism, which allows for the effects of fluid compressibility to dominate. These complementary effects lead to rich flow behavior and thus an intricate energy dissipation landscape.[19,20]

In this article, we provide the essential extension of these studies to the higher order vibrational modes of microfluidic beam devices. These modes are of critical importance in practice, since they allow for novel flow control of particulates and enhanced mass sensitivity, for example.[25] Knowledge of their dynamic characteristics is thus vital for future developments and the resulting interpretation of measurements. In contrast to conventional cantilever beams immersed in liquid, the quality factor of microfluidic beam devices typically decreases with increasing mode number.[16,25] The underlying physical mechanisms giving rise to this behavior are explored. Critically, we find that the effects of fluid compressibility are enhanced with increasing mode number. This leads to the aforementioned high viscosity pumping effects (for the fundamental mode) being exhibited at moderate to low viscosities in the higher order modes. Acoustic effects in the fluid are also found to be possible for operation in the higher order modes, in contrast to the fundamental mode that is immune from such effects. This results in resonant energy dissipation properties not experienced by the fundamental mode. The validity of these findings is assessed by comparison to detailed measurements as a function of fluid viscosity.

We begin by reviewing the underlying assumptions of the theoretical model of Refs. 19 and 20, and summarize its key formulas. This model is generalized to allow for evaluation at any mode number—provided the underlying assumptions remain valid, which we shall discuss. Second, we present a scaling analysis to explore the effect of increasing mode number, and investigate how this affects flow properties in the microfluidic channel. Examination of the case where the fluid channel is placed directly on the neutral axis of the beam is then discussed, and followed by off-axis channel placement away from the neutral axis. A comprehensive analysis and discussion of each case is given. Finally, a comparison to detailed measurements of the first and second modes over a wide range of fluid viscosities is presented, for which the theoretical model is found to be universally valid.

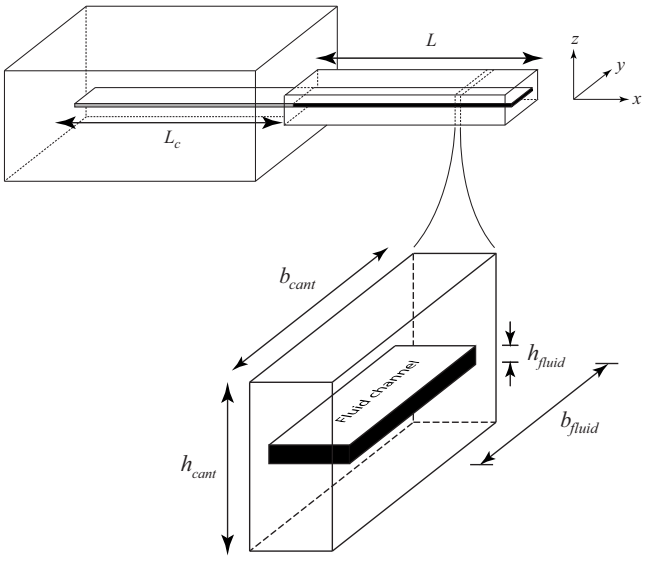

FIG. 2. Schematic illustration of rectangular cantilever ($x>0$) with embedded fluid channel and rigid lead channel ($x<0$) showing dimensions. Placement of the fluid channel away from the mid-plane (neutral axis) of the cantilever beam, in the z-direction, is specified by z_0. Origin of Cartesian coordinate system is center-of-mass of clamped end.

II. THEORETICAL MODEL

The principal aim of this article is to examine the effect of mode number on the quality factor of microfluidic beam devices. While results were given only for the fundamental mode of vibration in Refs. 19 and 20, the theoretical model presented in Ref. 20 is also applicable to higher order vibrational beam modes. This is provided the underlying assumptions of Euler–Bernoulli beam theory and the commensurate treatment of the fluid-structure problem, are maintained; see Ref. 20 for details. Application to higher order modes then simply requires use of the deflection function for each mode under consideration, as specified by Euler–Bernoulli beam theory.[26] This extension is specifically addressed in the following outline of the theoretical model. The dimensions of the device are illustrated in Fig. 2.

The theoretical model is derived under the following geometric assumptions:

(A) Cantilever length L is much larger than its width b_{cant} and thickness h_{cant};
(B) Fluid channel thickness h_{fluid} is much smaller than the channel width b_{fluid}—as a leading order approximation, we take the formal limit $h_{fluid}/b_{fluid} \to 0$ throughout;

(C) Fluid channel spans the entire length L of the cantilever;
(D) The lead channel of length L_c within the substrate of the chip is rigid;
(E) The amplitude of oscillation is much smaller than any geometric length scale of the beam so that the convective inertial term in the Navier–Stokes equation can be ignored and linear motion and flow is ensured.[9]

See Ref. 20 for a detailed discussion of the implications of these assumptions to practical devices. Next, we present a summary of key formulas required to calculate the quality factor using the theoretical model of Ref. 20. The quality factor of mode n is defined by

$$Q_n = 2\pi \left. \frac{E_{stored}}{E_{diss/cycle}} \right|_{\omega=\omega_{R,n}}, \tag{1}$$

where E_{stored} is the maximum energy stored in mode n, $E_{diss/cycle}$ is the energy dissipated per cycle in that mode, and $\omega_{R,n}$ is the radial resonant frequency of the mode. The principal equation for the quality factor of the microfluidic device due to the fluid only is

$$Q_n = F(\beta_n)\frac{\rho_{cant}}{\rho}\left(\frac{h_{cant}}{h_{fluid}}\right)\left(\frac{b_{cant}}{b_{fluid}}\right)\left(\frac{L}{h_{fluid}}\right)^2, \tag{2}$$

where for an arbitrary mode of vibration described by $\bar{W}_n(X)$, the normalized quality factor is given by

$$F(\beta_n) = \frac{\beta_n}{16\int_{-\bar{L}_c}^{1}\int_{-1/2}^{1/2}|G(X,Z)|^2 dZdX}, \tag{3a}$$

and

$$G(X,Z) = \left\{1 - \frac{1-i}{2}\sqrt{\frac{\beta_n}{2}}\frac{\cosh\left[(1-i)\sqrt{\frac{\beta_n}{2}}Z\right]}{\sinh\left(\frac{1-i}{2}\sqrt{\frac{\beta_n}{2}}\right)}\right\}\frac{d\bar{W}_n}{dX} + \frac{i\beta_n\bar{Z}_0}{2}\left\{\frac{\sinh\left[(1-i)\sqrt{\frac{\beta_n}{2}}Z\right]}{(1-i)\sqrt{\frac{\beta_n}{2}}\cosh\left(\frac{1-i}{2}\sqrt{\frac{\beta_n}{2}}\right) - 2\sinh\left(\frac{1-i}{2}\sqrt{\frac{\beta_n}{2}}\right)}\right\}$$
$$\times[S(X)-h(X)]\left.\frac{d\bar{W}_n}{dX}\right|_{X=1}, \tag{3b}$$

$$X = \frac{x}{L}, \quad Z = \frac{z-z_0}{h_{fluid}}, \quad \bar{Z}_0 = \frac{z_0}{h_{fluid}}, \quad \bar{L}_c = \frac{L_c}{L}. \tag{3c}$$

where $\bar{W}_n(X)$ is the normalized deflection function of a cantilever beam, such that $\bar{W}_n(1)=1$. Note that $\bar{W}_n(X)$ is specified by the Euler–Bernoulli beam equation[26] under clamped-free boundary conditions, the solution of which for arbitrary mode number n is

$$\bar{W}_n(X) = \frac{(-1)^n}{2}\left([\cos C_n X - \cosh C_n X] + \frac{\cos C_n + \cosh C_n}{\sin C_n + \sinh C_n}[\sinh C_n X - \sin C_n X]\right), \tag{4}$$

where C_n is the nth positive root of

$$\cosh C_n \cos C_n = -1. \tag{5}$$

The deflection functions for the first three modes, as specified by Eq. (4), are illustrated in Fig. 3.

Several dimensionless parameters appear in Eq. (3). The parameter β_n is defined by

$$\beta_n = \frac{\rho\omega_{R,n}h_{fluid}^2}{\mu}, \tag{6}$$

and is commonly referred to as the *Reynolds number*.[27] This parameter indicates the importance of fluid inertia, where ρ is the fluid density and μ is the fluid shear viscosity. The

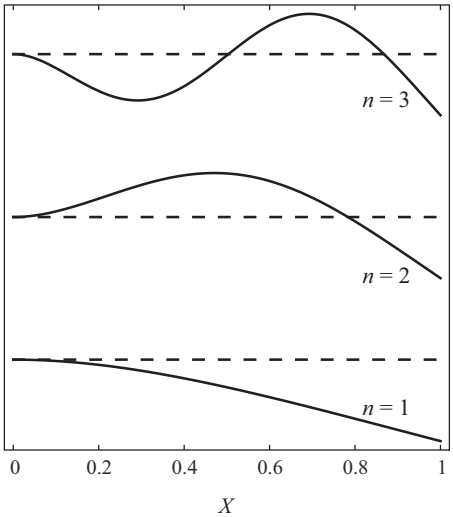

FIG. 3. Deflection function of first three modes of a cantilever beam. Arbitrary amplitude units on the vertical axis.

average density of the cantilever (with fluid) is specified by ρ_{cant}, and appears in Eq. (2).

Other dimensionless parameters in Eq. (3) are connected to compressibility of the fluid,

$$\gamma_n = \left(\frac{\omega_{R,n} L}{c}\right)^2, \quad \alpha_n = \frac{\gamma_n}{\beta_n}, \tag{7}$$

where γ_n is the *normalized wave number* and indicates the importance of acoustic effects, whereas α_n is related to the dilation of a fluid element due to compressibility and is termed the *compressibility number*. The speed of sound of the fluid is denoted c.

Additional functions required in Eq. (3) are

$$S(X) = \begin{cases} -1 + \dfrac{\dfrac{d\bar{W}_n}{dX}}{\left.\dfrac{d\bar{W}_n}{dX}\right|_{X=1}}: & 0 \le X \le 1 \\ -1: & -\bar{L}_c \le X < 0 \end{cases}, \tag{8a}$$

$$h(X) = -\frac{\alpha_n}{M\cos[M(1+\bar{L}_c)]}\left\{\sin[M(1-X)]\int_{-\bar{L}_c}^{X}[iBS(x') - \beta_n]\cos[M(x'+\bar{L}_c)]dx' + \cos[M(X+\bar{L}_c)]\int_{X}^{1}[iBS(x') - \beta_n]\sin[M(1-x')]dx'\right\}, \tag{8b}$$

where

$$B = \frac{-2i\beta_n \sinh\left(\dfrac{1-i}{2}\sqrt{\dfrac{\beta_n}{2}}\right)}{(1-i)\sqrt{\dfrac{\beta_n}{2}}\cosh\left(\dfrac{1-i}{2}\sqrt{\dfrac{\beta_n}{2}}\right) - 2\sinh\left(\dfrac{1-i}{2}\sqrt{\dfrac{\beta_n}{2}}\right)}, \tag{9a}$$

$$M = \sqrt{\alpha_n(\beta_n + iB)}. \tag{9b}$$

A complete description and derivation of the above model is given in Ref. 20, along with explicit results for the fluid velocity, energy dissipation and pressure distribution in the device for the fundamental mode of vibration.

III. RESULTS AND DISCUSSION

Next, we examine results arising from this theoretical model as a function of mode number n. We commence with a scaling analysis, which is followed by a detailed discussion complete with numerical results. Finally, a comprehensive comparison with experimental measurements on three separate devices over a wide range of fluids is presented.

A. Scaling behavior with mode number

Importantly, the resonant frequency increases with increasing mode number n, and is given by[26]

$$\omega_{R,n} = \frac{C_n^2}{L^2}\sqrt{\frac{EI}{\sigma}}, \tag{10}$$

where EI is the beam flexural rigidity, σ is its mass per unit length and L is the cantilever length. The coefficient C_n is specified by Eq. (5), and well approximated by

$$C_n \approx \frac{2n-1}{2}\pi, \quad n \ge 2. \tag{11}$$

As such, the dimensionless parameters specified in Eqs. (6) and (7) for arbitrary mode number n can be expressed in terms of parameters for the fundamental mode ($n=1$),

$$\beta_n = \left(\frac{C_n}{C_1}\right)^2\beta_1, \quad \gamma_n = \left(\frac{C_n}{C_1}\right)^4\gamma_1, \quad \alpha_n = \left(\frac{C_n}{C_1}\right)^2\alpha_1, \tag{12}$$

where the subscripts denote the mode number under consideration.

From Eq. (12), we observe that as the mode number n increases, all dimensionless parameters also increase. Since C_n increases approximately linearly with n [see Eq. (11)], the above scaling relations indicate a strong enhancement of inertial, acoustic and compressibility effects as mode number increases. Importantly, we find that the normalized wave number γ_n increases much more rapidly with increasing mode number n than other dimensionless parameters, indicating that acoustic effects are most strongly enhanced. The

practical implications of these findings will be discussed in detail in the following sections.

To begin, we consider the case where the fluid channel is placed directly on the neutral axis of the beam, i.e., $z_0=0$. This shall henceforth be termed *on-axis* channel placement.

B. On-axis channel placement

Here, the model simplifies dramatically and from Eq. (3) we obtain the following result for the normalized quality factor

$$F(\beta_n) = A_n \beta_n \left(16 \int_{-1/2}^{1/2} \left| 1 - \frac{1-i}{2} \sqrt{\frac{\beta_n}{2}} \frac{\cosh\left((1-i)\sqrt{\frac{\beta_n}{2}} Z \right)}{\sinh\left(\frac{1-i}{2} \sqrt{\frac{\beta_n}{2}} \right)} \right|^2 dZ \right)^{-1}, \tag{13a}$$

where

$$A_n = \left(\int_0^1 \left[\frac{d\bar{W}_n}{dX} \right]^2 dX \right)^{-1}. \tag{13b}$$

From Eq. (13), we observe decoupling of the fluid properties and deflection function, as characterized by the Reynolds number β_n, and mode parameter A_n, respectively. Varying the mode number n thus only rescales the magnitude of $F(\beta_n)$, leaving its functional dependence on β_n unaffected. The underlying mechanism for this decoupled behavior is the localized nature of the fluid flow for the on-axis problem—the fluid is driven only by the local rigid body displacement and rotation of the beam at a given value of X, i.e., position along the beam axis.

The mode parameter A_n decreases monotonically with increasing n, see Fig. 4, and for large n possesses the asymptotic form

$$A_n = \frac{4}{n^2\pi^2}, \quad n \to \infty, \tag{14}$$

which is also shown in Fig. 4. This feature results in an overall decrease in $F(\beta_n)$, and hence quality factor Q_n, with increasing mode number n at fixed β_n—the effect of varying β_n is examined below. The decrease in quality factor with increasing n is strong, varying as the inverse square of the mode number at large n; the effect is even stronger for small n.

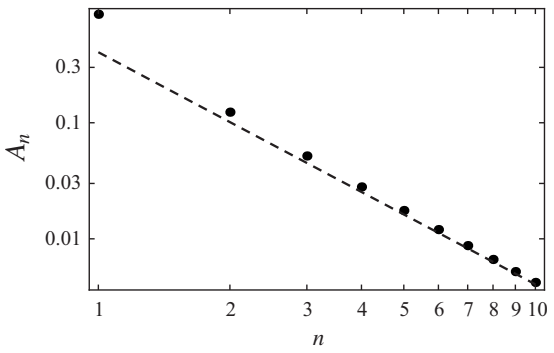

FIG. 4. Plot of mode parameter A_n as a function of mode number n. Exact solution (dots). Asymptotic solution for large n (dashed line).

This pronounced decrease in the quality factor is due to higher gradients in the deflection function along the beam length, which in turn drive the fluid motion; see Refs. 19 and 20. This enhances energy dissipation in the fluid and hence lowers the quality factor.

For comparison, conventional cantilevers immersed in fluid yield flows that are generated by the beam displacement rather than the displacement gradient[9,13]—this gives rise to the observed increase in quality factor with increasing mode number in those complementary systems.[9,10,13]

From Eq. (13), we find that in the limits of small and large β_n, the normalized quality factor has the asymptotic forms

$$F(\beta_n) = A_n \begin{cases} \dfrac{45}{\beta_n}: & \beta_n \ll 1 \\ \dfrac{1}{4}\sqrt{\dfrac{\beta_n}{2}}: & \beta_n \gg 1 \end{cases}. \tag{15}$$

As such, the quality factor decreases monotonically, reaches a minimum value, and then increases monotonically, as β_n increases. This is identical behavior to that reported for the fundamental mode in Ref. 20.

Importantly, the global minimum in $F(\beta_n)$ occurs at a single value of $\beta_n^{\min}=46.434$, regardless of the mode number n, at which point the normalized quality factor is $F(\beta_n^{\min}) = 2.1118 A_n$. This feature is illustrated in Fig. 5, where the normalized quality factor $F(\beta_n)$ for the first three modes is given.

Data in this figure allows for examination of how the quality factor varies with mode number n for a given device and fluid, while accounting for any variation in β_n due to increasing resonant frequency with mode number. For example, consider two separate devices whose fundamental modes possess Reynolds numbers in the low and high inertia

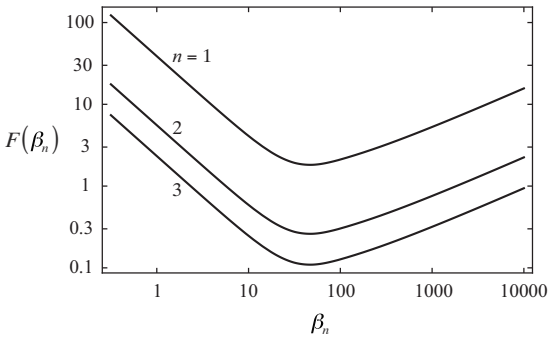

FIG. 5. Plot of normalized quality factor $F(\beta_n)$ as a function of β_n for the first three modes of vibration, $n=1,2,3$. Mode number n increases down the page.

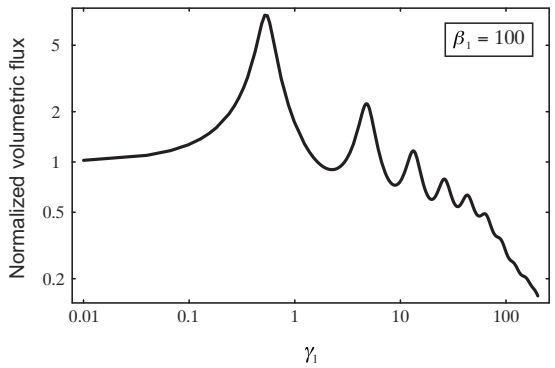

FIG. 6. Normalized magnitude of volumetric flux into rigid lead channel as a function of the normalized wave number γ_1 for fundamental mode with $\beta_1=100$. Volumetric flux scale is $q_s=u_s h_{fluid} b_{fluid}$ where $u_s=i\omega_{R,n} z_0 dW/dx|_{x=L}$ (Ref. 20).

regimes: $\beta_1=1$ and $\beta_1=100$, respectively. Using Eq. (12), we then find the following results for these two devices:

(1) $\beta_1=1$ device: first, second, and third modes exhibit normalized quality factors $F(\beta_1)=39$, $F(\beta_2)=0.91$, $F(\beta_3)=0.16$.
(2) $\beta_1=100$ device: first, second, and third modes exhibit normalized quality factors $F(\beta_1)=2.1$, $F(\beta_2)=0.62$, $F(\beta_3)=0.41$.

Since the material and geometric properties of the cantilever and hence normalization in Eq. (2) remain unchanged as the mode number n increases, these variations in the normalized quality factor $F(\beta_n)$ reflect true variations in the actual quality factor Q_n. As such, we find that a low inertia device exhibits a much stronger decrease in quality factor as the mode number increases, in comparison to a high inertia device. Significantly, the low and high inertia regimes can be achieved using small and large devices, respectively. We therefore conclude that small devices are more susceptible to strong reductions in quality factor with increasing mode number.

We emphasize, however, that these findings are for devices whose fluid channel is placed precisely on the neutral axis of the beam, i.e., $z_0=0$. Next, we examine the important practical case of off-axis channel placement ($z_0\neq 0$), which can dramatically affect the quality factor.[9,20]

C. Off-axis channel placement

Off-axis channel placement induces pumping of fluid into and out of the reservoir, due to net axial strain experienced by the fluid channel as the beam vibrates.[20] This enhances energy dissipation and hence lowers the quality factor. In Ref. 20 it was shown that this pumping mechanism dominates the on-axis flow only in the low inertia regime ($\beta_n<\beta_n^{\min}$), for typical devices operating in their fundamental mode. We now examine this behavior as a function of mode number n.

1. Acoustic resonances

Importantly, the effects of compressibility due to off-axis placement are enhanced with increasing mode number n, as discussed in Sec. III A. This can have a dramatic effect on the flow and hence the quality factor, as we now discuss. In Ref. 20, it was reported that acoustic resonances can occur in the off-axis flow; see Fig. 6. From Eq. (8b), the corresponding normalized wave numbers $\gamma_n=\bar{\gamma}_{n,m}$ at which these occur can be easily calculated in the asymptotic limit of high fluid inertia, i.e., $\beta_n\gg 1$:

$$\bar{\gamma}_{n,m}=\left[\frac{(2m-1)\pi}{2(1+\bar{L}_c)}\right]^2\left(1+\sqrt{\frac{2}{\beta_n}}\right)^{-1}. \tag{16a}$$

The corresponding acoustic resonance quality factor is

$$Q_{n,m}^{\text{acoustic}}=1+\sqrt{\frac{\beta_n}{2}}, \tag{16b}$$

where n is the mode number of the beam, and m is the order of the acoustic resonance. The first and second indices in both $\bar{\gamma}_{n,m}$ and $Q_{n,m}^{\text{acoustic}}$ thus refer to the orders of the beam mode and acoustic resonance, respectively.

Note that the quality factor $Q_{n,m}^{\text{acoustic}}$ is connected to the width of the acoustic resonance in wave number γ_n-space (see Fig. 6)—it is not the *quality factor* Q_n of the entire device that is in frequency ω-space. Importantly, from Eq. (16b) we find that the *acoustic quality factor* $Q_{n,m}^{\text{acoustic}}$ does not depend explicitly on the order m of the acoustic resonance, i.e., the "width" of each acoustic resonance is identical for fixed β_n. This salient feature is borne out in Fig. 6, where the width of each acoustic resonance peak appears similar on a logarithmic scale.

In the limit of zero viscous dissipation, i.e., $\beta_n\to\infty$, Eq. (16a) yields

$$\bar{\gamma}_{n,m}=\left[\frac{(2m-1)\pi}{2(1+\bar{L}_c)}\right]^2, \tag{16c}$$

which is simply the result for an inviscid acoustic standing wave in a rigid channel/cantilever system. Here, Eq. (16b) gives $Q_{n,m}^{\text{acoustic}}\to\infty$, thus yielding impulse functions for the acoustic resonances, as required.

Note that Eqs. (16) do not depend explicitly on the mode number n, with this dependence appearing implicitly via the Reynolds number β_n. This establishes that the position and width of the acoustic resonances in γ_n-space are independent

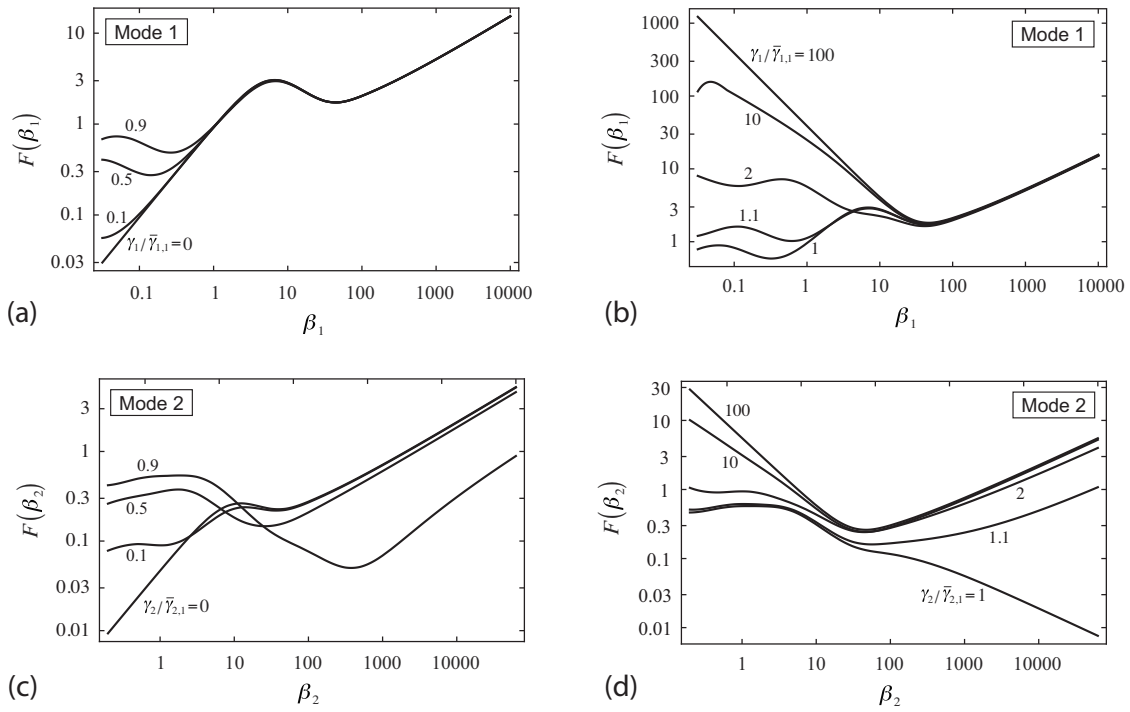

FIG. 7. Normalized quality factor $F(\beta_n)$ vs β_n for modes 1 and 2 showing variation as normalized wave number γ_n is varied around the critical values $\bar{\gamma}_{2,1}=(\pi/4)^2\approx 0.62$, which yields $\bar{\gamma}_{1,1}=\bar{\gamma}_{2,1}(C_1/C_2)^4\approx 0.016$; these values are calculated in the inviscid limit using Eq. (16c). Normalized wave number γ_n increases up the left hand side of each graph. Results for $\bar{Z}_0=0.1$.

of the deflection function of the mode, and arise from the geometry of the beam, its frequency of vibration and the fluid properties.

For the fundamental acoustic resonance $(m=1)$ of the fundamental beam mode $(n=1)$, Eq. (16c) yields normalized wave numbers of $\bar{\gamma}_{1,1}\sim O(1)$, as expected. Importantly, for the fundamental (beam) mode of practical devices, $\gamma_1 \ll \bar{\gamma}_{1,1}\sim O(1)$, and thus acoustic resonances cannot be manifest normally.

However, increasing the mode number n also increases the normalized wave number, γ_n, since the frequency of vibration is enhanced; see Eq. (12). Consequently, fluid flow generated by higher order vibrational modes of the beam can be strongly affected by acoustic effects, with a commensurate variation in the quality factor Q_n. Operation at one of the acoustic resonances of the off-axis flow can result in a strong increase in the volumetric flux into the fluid channel from the reservoir. This increases the velocity gradients in the channel and thus results in a strong enhancement in energy dissipation, i.e., reduction in quality factor Q_n. Critically, this acoustic resonance behavior only exists provided viscous damping is not strong, i.e., $\beta_n \gg 1$, otherwise the system is over damped.

In Fig. 7, we present results for a typical microfluidic cantilever device operating in modes 1 and 2, whose rigid lead channel is of identical length to the cantilever section, i.e., $\bar{L}_c=1$. A value of γ_1 (for mode 1) is chosen so that mode 2 operates at its fundamental acoustic resonance $(m=1)$. From Eq. (16c), which corresponds to the inviscid limit, the fundamental acoustic mode $(m=1)$ resonance of beam mode 2 $(n=2)$ occurs at $\bar{\gamma}_{2,1}=(\pi/4)^2\approx 0.62$, which yields $\bar{\gamma}_{1,1}=\bar{\gamma}_{2,1}(C_1/C_2)^4\approx 0.016$; these are excellent approximations for high β_n. The value of the normalized wave number γ_n is also swept around this value in Fig. 7. The lower-most curves in Figs. 7(a) and 7(c) correspond to the incompressible solutions $(\gamma_n=0)$, whereas the upper-most curves in Figs. 7(b) and 7(d) correspond to infinite compressibility $(\gamma_n\to\infty)$. The latter case eliminates any effect due to off-axis placement of the fluid channel—the volumetric flux into the channel is zero, since the fluid simply dilates as the channel extends and contracts along its axis.

Next, we examine how increasing the mode number n affects energy dissipation. We remind the reader that fluid compressibility and acoustic effects manifest themselves only in the off-axis flow problem.[20] We therefore focus our discussion on energy dissipation arising from this off-axis problem, while presenting complete numerical results that incorporate both on-axis and off-axis flow mechanisms.

2. Fundamental beam mode (mode 1)

From Figs. 7(a) and 7(b) it is evident that for mode 1 of the cantilever beam $(n=1)$, increasing the normalized wave number γ_1 increases the normalized quality factor monotonically for nearly all values of Reynolds number β_1. Since finite compressibility allows the fluid to dilate, the volumetric flux into the channel induced by the off-axis pumping mechanism decreases. This reduces the shear velocity gradients and hence energy dissipation, resulting in an increase in quality factor in comparison to the incompressible case. Importantly, we find that the off-axis flow has very little effect on the quality factor for $\beta_1 > \beta_1^{\min}=46.434$, where the on-axis flow problem dominates energy dissipation, as was reported in Ref. 20.

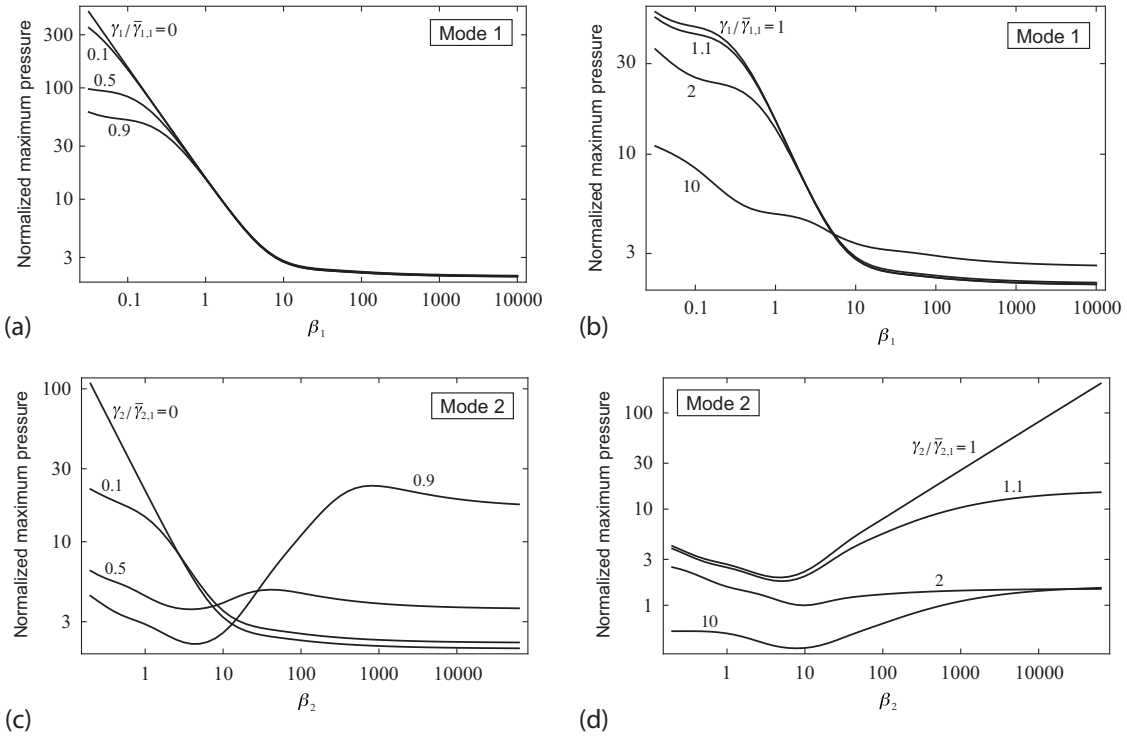

FIG. 8. Normalized maximum pressure $|\bar{P}_{\max}|$ vs β_n for modes 1 and 2 showing variation as normalized wave number γ_n is varied around the critical values $\bar{\gamma}_{2,1}=(\pi/4)^2\approx 0.62$, which yields $\bar{\gamma}_{1,1}=\bar{\gamma}_{2,1}(C_1/C_2)^4\approx 0.016$; these values are calculated in the inviscid limit using Eq. (16c). Results for $\bar{Z}_0=0.1$. Pressure scale is $P_s=\rho\omega_{R,n}u_sL$ where $u_s=i\omega_{R,n}z_0dW/dx|_{x=L}$, and is appropriate for the high inertia incompressible regime (Ref. 20).

3. Second beam mode (mode 2)

The behavior for mode 2 of the beam ($n=2$) differs greatly from that observed for mode 1; cf. Figs. 7(a) and 7(c) and Figs. 7(b) and 7(d). As fluid compressibility increases from zero ($\gamma_2=0$), we observe an enhancement in the quality factor Q_2 for $\beta_2<\beta_2^{\min}=46.434$, similar to the fundamental mode. However, we now find that the quality factor can also be strongly affected in the high inertia region $\beta_2>\beta_2^{\min}=46.434$—this coincides with the region where acoustic resonance effects occur, which were discussed above. The result is a dramatic decrease in the quality factor Q_2 near the fundamental acoustic resonance of mode 2, i.e., $\gamma_2=\bar{\gamma}_{2,1}\sim(\pi/4)^2\approx 0.62$. This feature is due to strong enhancement of the volumetric flux into the device, which greatly enhances viscous dissipation. Note that at the acoustic resonance point $\gamma_2=\bar{\gamma}_{2,1}\sim(\pi/4)^2\approx 0.62$, the quality factor decreases with increasing β_2, in stark contrast to the on-axis (incompressible) solution that displays the reverse behavior.

Physically, an increase in β_2 can be realized by decreasing the fluid viscosity. We thus find the apparently unintuitive result that a decrease in viscosity enhances energy dissipation, i.e., the quality factor decreases. This phenomenon is due to competition between a strong enhancement in the volumetric flux into the device near the acoustic resonance, and a reduction in viscosity. The increase in volumetric flux enhances the shear velocity gradients, which dominates other effects, and results in a strong increase in the total energy dissipation.

Increasing the mode number thus allows for excitement of acoustic resonances, which can strongly modify the energy dissipation landscape, particularly at high inertia; in the low inertia regime, acoustic resonances are over damped and hence not significant. We emphasize that this acoustic effect differs to nonacoustic (quasistatic) dilational compressibility effects reported for the fundamental mode $n=1$ (see Sec. III C 2), which are prevalent in the low inertia regime.

4. Maximum pressure

The presence of acoustic resonances can also dramatically enhance the pressure within the fluid channel. In Fig. 8, we present results for the maximum pressure in the channel due to the off-axis pumping mechanism, at the operating conditions considered in Fig. 7; pressure contribution from the off-axis flow problem dominates that from the on-axis flow.[20] For mode 1, we observe a monotonic change in the maximum pressure as the normalized wave number increases; see Figs. 8(a) and 8(b). This is to be expected, since this beam mode operates well below the fundamental acoustic resonance of the device. In contrast, from Figs. 8(c) and 8(d) we observe that mode 2 exhibits a striking enhancement in the maximum pressure as the fundamental acoustic resonance is approached, i.e., $\gamma_2=\bar{\gamma}_{2,1}$. This enhancement increases with increasing Reynolds number β_2, since (i) the acoustic quality factor, $Q_{2,1}^{\text{acoustic}}$, is also enhanced in this situation, i.e., the acoustic resonance becomes more under damped, and (ii) the acoustic resonance condition used in the results, as specified in Eq. (16c), is for zero damping, i.e., $\beta_2\to\infty$.

To illustrate the strong enhancement in pressure due to acoustic resonance effects, consider the case of $\beta_2=1000$. From Figs. 8(c) and 8(d), we find that the maximum pressure increases by a factor of ~ 10 as the normalized wave number

TABLE I. Dimensions and beam resonance properties for three devices used in comparison. Resonant frequencies are given for air. The specified fluid channel width is the sum of both parallel channel widths in the actual devices, as required in the theoretical model.

	Dimensions (μm)						Resonances			
							Mode 1		Mode 2	
Device	h_{fluid}	b_{fluid}	h_{cant}	b_{cant}	L	L_c	f_1^{res} (kHz)	Q_1^{air}	f_2^{res} (kHz)	Q_2^{air}
A	3	16	7	33	210	207.5	218.9	17 919	1354.1	7092
B	8	16	12	33	210	207.5	411.6	8 583	2476.0	4739
C	15	40	19	57	321	240	275.1	4 068	1663.9	5093

increases from $\gamma_2=0.5\bar{\gamma}_{2,1}$ to $\gamma_2=\bar{\gamma}_{2,1}$. In contrast, as γ_2 increases further from $\gamma_2=\bar{\gamma}_{2,1}$ to $\gamma_2=2\bar{\gamma}_{2,1}$ the maximum pressure displays a strong reduction by a factor of ~15. Such clear resonance behavior is totally absent in mode 1, which always operates in the quasistatic (nonacoustic) regime. These results serve to illustrate the potential of higher order beam modes to enhance the maximum pressure, which may be important in applications where cavitation or other high-pressure phenomena may be desirable. See Ref. 20 for a discussion of the potential importance of such modes of operation.

Operation in beam modes higher than mode 2 yields similar results to the above, since such acoustic mechanisms are identical.

D. Experimental measurements

We now present a detailed comparison of the above theoretical model to measurements on a series of microfluidic cantilever devices. Three devices are chosen for this comparison, whose dimensions allow for both low and high inertia regimes to be probed. The geometric and mechanical properties of these cantilevers are given in Table I. Measurements were taken using a glycerol/water mixture, allowing for the viscosity to be varied over three orders of magnitude; mixtures ranging from pure water to 96% glycerol (by weight) were utilized. A fixed pressure difference of ~34.5 kPa was applied across the inlets of the microfluidic channel in all measurements, resulting in a constant (steady) flow rate; increasing viscosity reduced the flow rate. Varying this pressure difference had negligible effect on measurements of the frequency response. A wash step was performed between measurements on different fluids, for which the pressure was increased to a fixed value ~103 kPa for all fluids. The resonant frequencies and quality factors of modes 1 and 2 of these devices with air and glycerol/water mixtures in the fluid channel are given in Table I and Fig. 9. Measure-

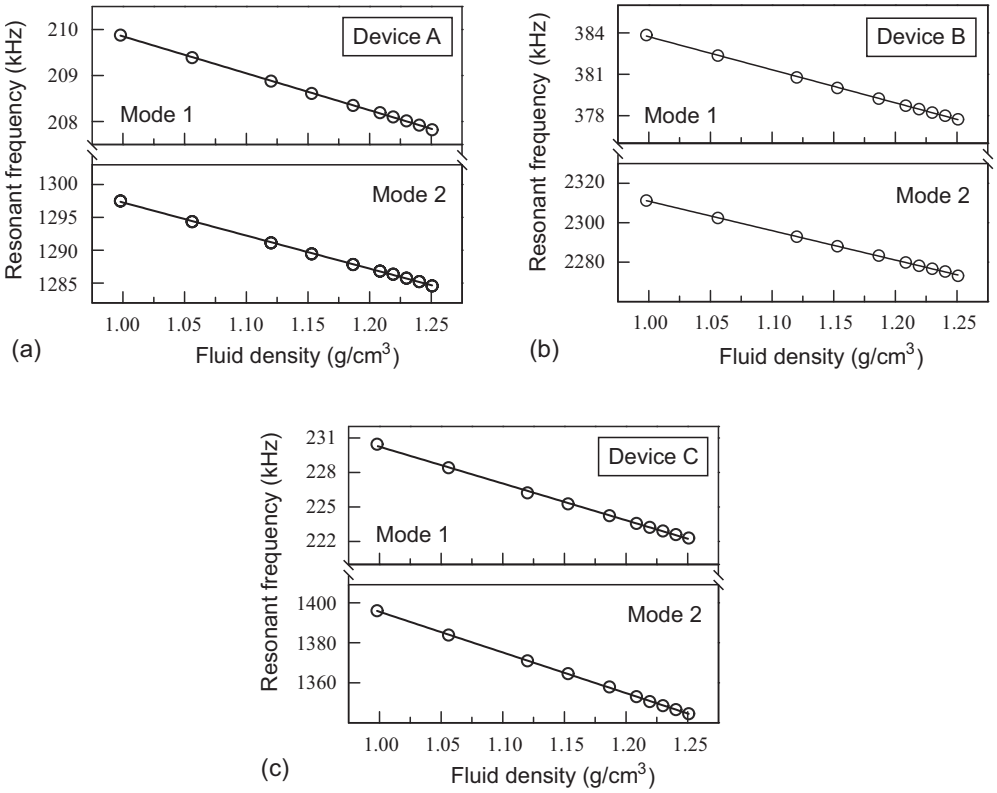

FIG. 9. Measured resonant frequencies of devices for modes 1 and 2 as a function of liquid density. Similar frequency sensitivities are obtained for modes 1 and 2 for a single device. Frequency sensitivities for modes 1, 2: Device A $(3.83\pm0.02,\ 3.88\pm0.03)$ %/g/cm^{-3}; Device B $(6.24\pm0.05,\ 6.45\pm0.03)$ %/g/cm^{-3}; Device B $(13.89\pm0.16,\ 14.57\pm0.06)$ %/g/cm^{-3}. Percentage frequency shifts relative to that in water given.

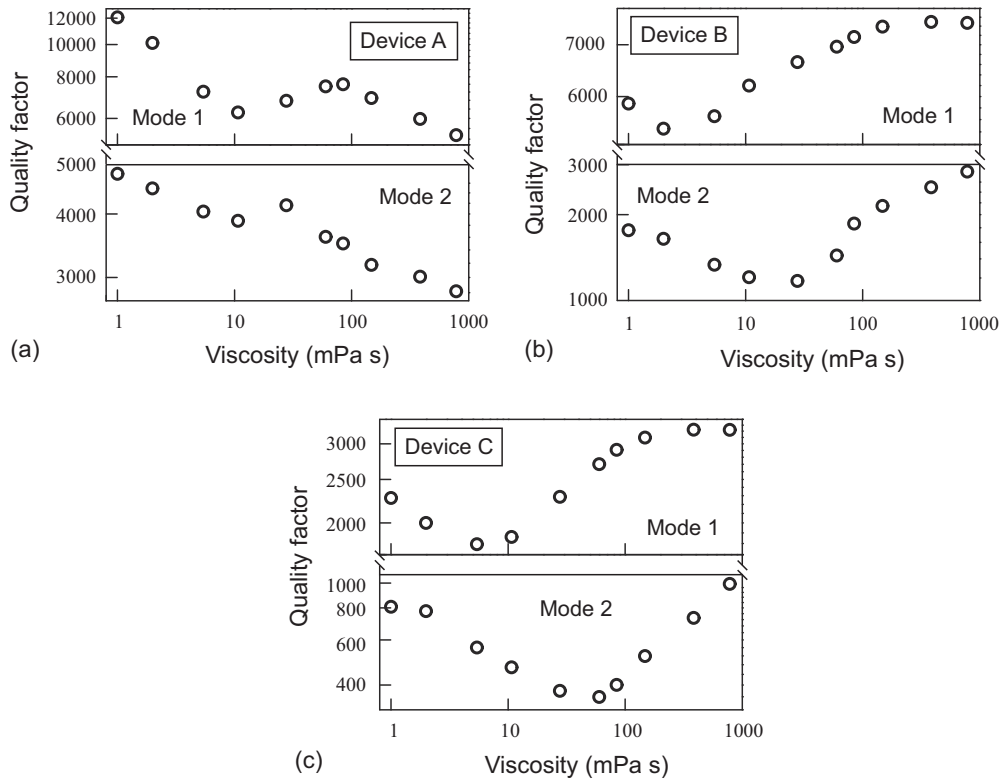

FIG. 10. Measured quality factors of devices for modes 1 and 2 as a function of liquid viscosity. A glycerol/water mixture is used to vary the viscosity—the density also varies slightly with viscosity for this reason. Logarithmic scales used for all axes.

ment of beam modes higher than the second was not possible due to technical limitations.

1. Preliminary discussion

To begin, we examine dependence of the resonant frequency on liquid density. Importantly, the resonant frequency is expected to depend primarily on fluid density since the net force exerted by the fluid on the cantilever, in the cantilever direction of motion (z-direction; see Fig. 2), is insensitive to viscosity[20]—the effective mass of the cantilever is therefore insensitive to viscosity, within the framework of Euler-Bernoulli beam theory. This contrasts to a conventional microcantilever immersed in fluid, whose resonant frequency depends strongly on fluid viscosity.[9] This feature of microfluidic beam resonators is borne out in measurements of the resonant frequency for various glycerol/water mixtures, where all devices show excellent linear dependence on liquid density; see Fig. 9—this behavior is in the presence of a viscosity change spanning three orders of magnitude. The resonant frequency sensitivities of modes 1 and 2 for each device are also similar, with the slight differences consistent with the fluid channel not spanning the full length of the cantilever beam; see Fig. 1. These results indicate that the devices perform as expected.

In contrast, the measured quality factors display a striking nonmonotonic dependence on liquid viscosity, as was previously reported for the fundamental mode;[20] see Fig. 10. Interestingly, mode 2 is found to exhibit lower quality factors than those found for the fundamental mode (mode 1), in qualitative agreement with predictions of the theoretical model; see Sec. III B. Furthermore, we also note that maxima and minima in the quality factors for modes 1 and 2 appear to be displaced along the viscosity axis. This behavior is in stark contrast to the resonant frequency, which exhibits a simple linear variation, cf. Figs. 9 and 10.

Before making a quantitative comparison between the measured quality factors in Fig. 10 and numerical results of the theoretical model, we present some general observations regarding the hydrodynamic regimes in which these devices operate. Values for the three dimensionless variables of each device are given in Tables II and III, for water in the fluid channel.

Results for the fundamental mode (mode 1) are presented in Table II, where we observe that all three devices operate in the low to high inertia regime—Reynolds number $14 < \beta_1^{water} < 378$. Increasing the viscosity of the liquid through addition of glycerol reduces the Reynolds number β_1 and hence decreases inertial effects. Importantly, we find that the normalized wave numbers of all devices lie well below those of the predicted fundamental acoustic resonances for each device, i.e., $\gamma_1^{water} \ll \bar{\gamma}_{1,1}$; compare italicized numbers in Table II. Since (i) the addition of glycerol increases the speed of sound (decreases the compressibility), and (ii) the normalized wave numbers are inversely proportional to the square of the sound speed, this then establishes that acoustic effects are totally absent in all three devices when operated in their fundamental modes. Finally, we note that the compressibility numbers α_1^{water} are small (for water). However, by adding glycerol to the solution, these values can be substantially increased and approach unity. This indicates that compress-

TABLE II. Mode 1 device parameters for water. Dimensionless parameters of measured devices along with theoretical predictions of acoustic resonances. Note that all devices operate well below the expected acoustic resonances (compare italicized numbers), i.e., $\gamma_1^{water} \ll \bar{\gamma}_{1,1}$.

	Mode 1				
	Experimental dimensionless parameters			Theoretical acoustic resonance $n=1$, $m=1$	
Device	β_1^{water}	γ_1^{water}	α_1^{water}	$\bar{\gamma}_{1,1}$	$Q_{1,1}^{\text{acoustic}}$
A	14	*0.034*	0.002 5	*0.29*	3.6
B	179	*0.11*	0.000 64	*0.47*	10
C	378	*0.096*	0.000 25	*0.67*	15

ibility effects are not important for water but can strongly affect the flow for a glycerol/water mixture of high glycerol concentration.

From Table III, it is clear that operation in mode 2 strongly enhances the effects of compressibility, while also increasing fluid inertia. Note that the Reynolds numbers, β_2^{water}, in Table III (for mode 2) are approximately an order of magnitude larger than those in Table II (for mode 1)—the devices now operate in the moderate to very high inertia regime. This is due to the increase in resonant frequencies in going from mode 1 to mode 2. Second, we find that acoustic effects may now reveal themselves strongly in mode 2 of all devices, with all normalized wave numbers, γ_2^{water}, lying between the fundamental and next higher harmonic acoustic resonances of the devices—compare the italicized numbers in Table III. Note that the normalized wave numbers are weakly affected as the glycerol/water concentration is varied—they decrease by at most a factor of ~2 as the glycerol concentration is enhanced, due to the increase in sound speed. Even so, we observe that none of these devices operate directly at the predicted acoustic resonances, i.e., $\gamma_2 \neq \bar{\gamma}_{2,1}$, $\bar{\gamma}_{2,2}$. Furthermore, the large acoustic quality factors $Q_{2,1}^{\text{acoustic}}$ establish that operation in the immediate vicinity of the acoustic resonances is required for manifestation of substantial acoustic resonance effects. Such acoustic effects are thus not expected to present themselves in these devices. Finally, the compressibility numbers, α_2^{water}, are found to be an order of magnitude larger than those for the fundamental mode (mode 1). As such, dilational effects due to compressibility in the off-axis flow are expected to be even stronger for mode 2. However, since fluid inertia is large for mode 2 and acoustic effects are absent, this can weaken such dilational compressibility effects because the on-axis flow dominates in this high inertia regime. This will be examined in detail below.

2. Quantitative comparison to theoretical model

With this initial discussion in hand, we now present a quantitative comparison of the measured normalized quality factor $F(\beta_n)$ to the theoretical model, Eq. (3a). The experimental normalized quality factors $F(\beta_n)$ were obtained from measurements of the quality factors Q_n, using Eq. (2). These values were then compared to theoretical predictions. Speeds of sound of the water/glycerol mixtures vary linearly with mass fraction,[28] and were calculated accordingly in the theoretical model. Theoretically, the only unknown parameter in the model is the off-axis placement of the fluid channel, $\bar{Z}_0$—this was used as a fitting parameter.[20] Since $\bar{Z}_0$ is a fixed geometric property of each device, its value cannot vary between mode number. As such, $\bar{Z}_0$ was obtained by fitting results for the fundamental mode only of each device; theoretical results for mode 2 were then calculated using this fixed value. This provides a further consistency check and assessment on the validity of the theoretical model.

a. Fundamental beam mode (mode 1). Results for the fundamental mode normalized quality factors $F(\beta_1)$ of each device are given in Fig. 11, where a quantitative comparison between theory and measurement is presented. Corresponding values for the fitted off-axis placement, $\bar{Z}_0$, of the fluid channel are given in the caption; these are obtained from fits to the fundamental beam mode only of each device, as discussed above. Theoretical results are given for the (full) theoretical model that includes the effects of compressibility, and results in the incompressible limit. Note the good agree-

TABLE III. Mode 2 device parameters for water. Dimensionless parameters of measured devices along with theoretical predictions of acoustic resonances. Note that devices operate above the expected fundamental acoustic resonance $m=1$ but are in the vicinity of the second acoustic resonance $m=2$ (compare italicized numbers), i.e., $\gamma_2^{water} \sim \bar{\gamma}_{2,2}$.

	Mode 2						
				Theoretical acoustic resonances $n=2$			
	Experimental dimensionless parameters			$m=1$		$m=2$	
Device	β_2^{water}	γ_2^{water}	α_2^{water}	$\bar{\gamma}_{2,1}$	$Q_{2,1}^{\text{acoustic}}$	$\bar{\gamma}_{2,2}$	$Q_{2,2}^{\text{acoustic}}$
A	85	*1.3*	0.015	*0.42*	7.5	*3.8*	7.5
B	1078	*4.1*	0.0038	*0.55*	24	*4.9*	24
C	2291	*3.5*	0.0015	*0.74*	35	*6.6*	35

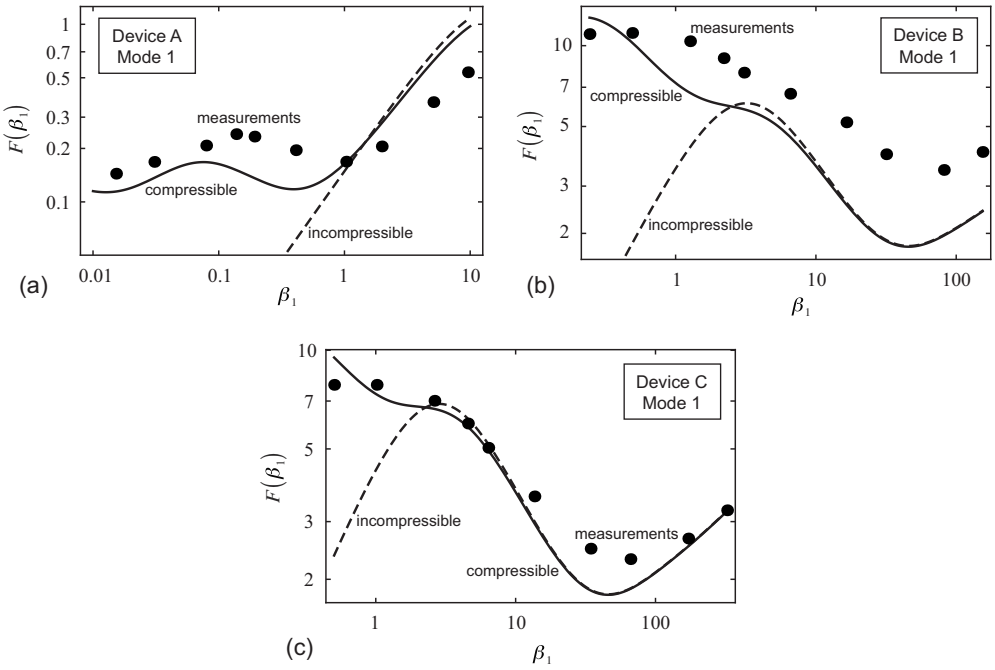

FIG. 11. Fundamental mode (mode 1). Comparison of theoretical model (lines) to measurements (solid circles) for devices A, B, C. Off-axis placement for each device: A ($\bar{Z}_0$=0.25); B ($\bar{Z}_0$=0.05); C ($\bar{Z}_0$=0.05). Solid line (compressible). Dashed line (incompressible).

ment between the full compressible theory and measurements, for all devices; the incompressible solution does not describe measurements well in the high viscosity (low inertia) regime. Devices A and B are of the same types as those studied in Refs. 19 and 20. Similarities between the results in Figs. 11(a) and 11(b) and Refs. 19 and 20 are notable, and for a possible explanation of the discrepancies between experiment and theory, the reader is referred to Ref. 20. Device C is new, and the agreement between the full compressible theory and measurement is also good. This device possesses a large channel thickness, and thus operates in the highest inertial regime. The minimum in the quality factor at $\beta \approx 46$ due to the on-axis flow is clearly visible in devices B and C; device A operates in an inertial regime below this expected minimum. Note that in all cases, consideration of fluid compressibility is essential in predicting the overall measured responses.

b. Second beam mode (mode 2). Next, we turn our attention to the second mode (mode 2) for which comparisons between theory and measurement are given in Fig. 12. The striking agreement between the full compressible theoretical

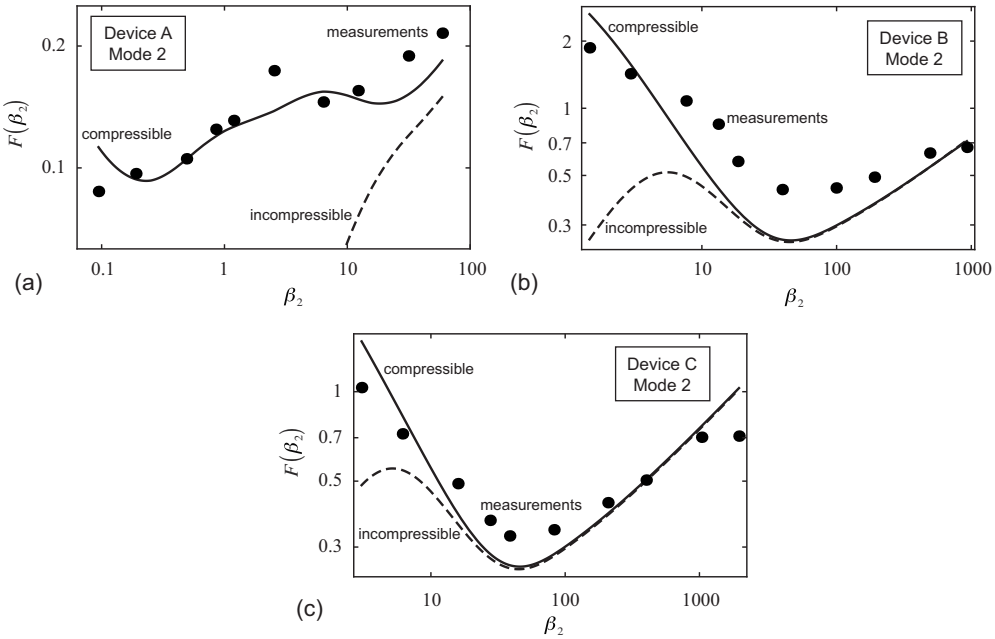

FIG. 12. Second mode (mode 2). Comparison of theoretical model (lines) to measurements (circles) for devices A, B, C. Off-axis placement for each device: A ($\bar{Z}_0$=0.25); B ($\bar{Z}_0$=0.05); C ($\bar{Z}_0$=0.05). Solid line (compressible). Dashed line (incompressible).

model and measurements provides further verification of the validity of the model. We again emphasize that the off-axis placements, $\bar{Z}_0$, are identical to those used for the fundamental mode, and are thus independent of measurements for mode 2. The dramatic decrease in the measured quality factors of the second mode in comparison to the fundamental mode for all devices (see Fig. 10), is also accurately predicted by the (full) compressible model (see Fig. 12). The theoretical model thus naturally accommodates these variations.

For device A, we find that fluid compressibility is essential in predicting the measured response; see Fig. 12(a). Unlike the fundamental mode, the incompressible model does not accurately predict measurements over any β_2-range, yielding a gross underestimate of the quality factor; the incompressible model diverges strongly away from the measured results in Fig. 12(a). Note that the effects of compressibility are vital even for water, which contrasts strongly to the fundamental mode. This is expected, since (i) compressibility effects are strong for the fundamental mode and are enhanced by increasing the mode number, and (ii) both modes 1 and 2 operate in the moderate to low inertia regimes, thus ensuring that the off-axis flow (which contains the compressibility effects) dominates the response. The expected minimum in the quality factor at $\beta_2 \approx 46$ is not observed for mode 2, however, since the off-axis channel placement is very large. Thus, off-axis effects spill over into the higher inertia regime and eliminate the expected minimum due to the on-axis flow.

For device B, we also find good agreement between theory and measurement; see Fig. 12(b). In the discussion above, it was theoretically predicted that the minimum in quality factor in β_n-space (due to the on-axis flow) is independent of mode number n. In agreement with this prediction, we find a minimum at $\beta_2 \approx 46$ for mode 2. This feature explains the displaced nature of the (true) quality factor Q_n versus viscosity data in Fig. 10; the minimum in the true quality factor occurs at a higher viscosity for mode 2 in comparison to mode 1—see Fig. 10(b). Compressibility effects are also important for mode 2 of this device but only in the low inertia regime, i.e., at the highest fluid viscosities. This is due to higher inertial effects in this device, which serve to weaken the influence of the off-axis (compressible) flow unless acoustic effects are presented; see discussion of theoretical model in Sec. III C. This also provides evidence for the absence of acoustic effects, which would be manifest by a decrease in the quality factor with increasing Reynolds number β_2, at high β_2; see Fig. 7(d).

Device C exhibits similar behavior to device B, with a minimum in the normalized quality factor occurring at the expected value of $\beta_2 \approx 46$ for mode 2; see Fig. 12(c). This accurately accounts for the displaced minimum in the true quality factor with respect to viscosity, as was observed for device B; cf. Figs. 10(c) and 12(c). The effects of compressibility are also present at low inertia, and are essential to predicting the response in this regime.

In summary, all variations in the measured quality factors of devices A, B, C are naturally captured by the full compressible theoretical model, which yields self-consistent predictions for both modes 1 and 2.

IV. CONCLUSIONS

We have examined the effect of mode number on energy dissipation in microfluidic beam resonators. In contrast to conventional cantilevers immersed in fluid, these devices typically exhibit a reduction in quality factor with increasing mode number. The underlying physical mechanism driving this feature is larger displacement gradients in the higher order beam modes, which enhance energy dissipation. Furthermore, it was found that the effects of fluid compressibility are also enhanced in the higher order modes. This leads to the possibility of probing acoustic resonances of the device, which can dramatically decrease the quality factor and enhance the maximum pressure. Finally, a detailed comparison between the theoretical model and experimental measurements on a range of devices was presented. These measurements span the low to high inertia regimes. Good agreement was found in all cases, thus demonstrating the validity and robust nature of the theoretical model. These results are expected to be of particular value in future developments that focus on higher order beam modes of oscillation for novel applications, such as enhanced mass sensitivity and flow control of particulates.[25]

ACKNOWLEDGMENTS

This work was supported by the Institute for Collaborative Biotechnologies through Contract No. W911NF-09–D-0001 from the U.S. Army Research Office, the NIH Cell Decision Process Center P50–GM68762, and by the Australian Research Council Grants Scheme.

[1] H. G. Craighead, Science **290**, 1532 (2000).
[2] K. L. Ekinci and M. L. Roukes, Rev. Sci. Instrum. **76**, 061101 (2005).
[3] N. V. Lavrik, M. J. Sepaniak, and P. G. Datskos, Rev. Sci. Instrum. **75**, 2229 (2004).
[4] F. J. Giessibl, Rev. Mod. Phys. **75**, 949 (2003).
[5] Y. T. Yang, C. Callegari, X. L. Feng, K. L. Ekinci, and M. L. Roukes, Nano Lett. **6**, 583 (2006).
[6] K. Jensen, K. Kim, and A. Zettl, Nat. Nanotechnol. **3**, 533 (2008).
[7] H.-Y. Chiu, P. Hung, H. W. Ch. Postma, and M. Bockrath, Nano Lett. **8**, 4342 (2008).
[8] H.-J. Butt, P. Siedle, K. Seifert, K. Fendler, T. Seeger, E. Bamberg, A. L. Weisenhorn, K. Goldie, and A. Engel, J. Microsc. **169**, 75 (1993).
[9] J. E. Sader, J. Appl. Phys. **84**, 64 (1998).
[10] T. Braun, V. Barwich, M. K. Ghatkesar, A. H. Bredekamp, Ch. Gerber, M. Hegner, and H. P. Lang, Phys. Rev. E **72**, 031907 (2005).
[11] M. Pelton, J. E. Sader, J. Burgin, M. Liu, P. Guyot-Sionnest, and D. Gosztola, Nat. Nanotechnol. **4**, 492 (2009).
[12] C. Castille, I. Dufour, and C. Lucat, Appl. Phys. Lett. **96**, 154102 (2010).
[13] C. A. Van Eysden and J. E. Sader, J. Appl. Phys. **101**, 044908 (2007).
[14] C. A. Van Eysden and J. E. Sader, J. Appl. Phys. **106**, 094904 (2009).
[15] T. P. Burg, M. Godin, S. M. Knudsen, W. Shen, G. Carlson, J. S. Foster, K. Babcock, and S. R. Manalis, Nature (London) **446**, 1066 (2007).
[16] J. Lee, W. Shen, K. Payer, T. P. Burg, and S. R. Manalis, Nano Lett. **10**, 2537 (2010).
[17] J. W. M. Chon, P. Mulvaney, and J. E. Sader, J. Appl. Phys. **87**, 3978 (2000).
[18] K. Y. Yasumura, T. D. Stowe, E. M. Chow, T. Pfafman, T. W. Kenny, B. C. Stipe, and D. Rugar, J. Microelectromech. Syst. **9**, 117 (2000).
[19] T. P. Burg, J. E. Sader, and S. R. Manalis, Phys. Rev. Lett. **102**, 228103 (2009).

[20]J. E. Sader, T. P. Burg, and S. R. Manalis, J. Fluid Mech. **650**, 215 (2010).
[21]M. R. Paul and M. C. Cross, Phys. Rev. Lett. **92**, 235501 (2004).
[22]S. Basak, A. Raman, and S. V. Garimella, J. Appl. Phys. **99**, 114906 (2006).
[23]R. J. Clarke, S. M. Cox, P. M. Williams, and O. E. Jensen, J. Fluid Mech. **545**, 397 (2005).
[24]T. Naik, E. K. Longmire, and S. C. Mantell, Sens. Actuators, A **102**, 240 (2003).
[25]J. Lee, A. K. Bryan, and S. R. Manalis, Rev. Sci. Instrum. (to be published).
[26]S. Timoshenko and D. H. Young, *Elements of Strength of Materials* (D. Van Nostrand, New York, 1968).
[27]This parameter is often referred to under different names, e.g., Reynolds, inverse Stokes or Womersley number.
[28]L. Elvira-Segura, IEEE Trans. Ultrason. Ferroelectr. Freq. Control **48**, 632 (2001).